An open-source quadrature-based population balance solver for OpenFOAM

Alberto Passalaqua, Frédérique Laurent, E. Madadi-Kandjani, J C Heylmun, Rodney O Fox

An open-source quadrature-based population balance solver for OpenFOAM

A. Passalacqua[a,1,*], F. Laurent[b,c,1], E. Madadi-Kandjani[a], J. C. Heylmun[a], R. O. Fox[d]

[a]*Department of Mechanical Engineering, Iowa State University, Black Engineering Building, Ames, IA 50011, USA*
[b]*Laboratoire EM2C, CNRS, CentraleSupélec, Université Paris-Saclay, Grande Voie des Vignes, 92295 Châtenay-Malabry cedex, France*
[c]*Fédération de Mathématiques de l'Ecole Centrale Paris, FR CNRS 3487, France*
[d]*Department of Chemical and Biological Engineering, Iowa State University, Sweeney Hall, Ames, IA, 50011-2230, USA*

Abstract

The extended quadrature method of moments (EQMOM) for the solution of population balance equations (PBE) is implemented in the open-source computational fluid dynamic (CFD) toolbox OpenFOAM as part of the OpenQBMM project. The moment inversion procedure was designed (Nguyen et al., 2016) to maximize the number of conserved moments in the transported moment set. The algorithm is implemented in a general structure to allow the addition of other kernel density functions defined on $\mathbb{R}^+$, and arbitrary kernels to describe physical phenomena involved in the evolution of the number density function. The implementation is verified with a set of zero-dimensional cases involving aggregation and breakage problems. Comparison to the rigorous solution of the PBE provides validation for these cases. The

*Corresponding author
Email address: albertop@iastate.edu (A. Passalacqua)
[1]Equal contribution.

coupling of the EQMOM procedure with a CFD solver to address aggregation and breakage problems of non-inertial particles is validated against experimental measurements in a Taylor-Couette reactor from literature.
Keywords: Extended quadrature method of moments, log-normal kernel density function, population balance equation, aggregation and breakage, OpenFOAM, OpenQBMM

---

1. Introduction

The spatial and temporal evolution of a discrete population of particles can be described by a population balance equation (PBE) (Ramkrishna, 2000), which is an evolution equation for the number density function (NDF) associated to the particle population. The NDF can evolve due to discontinuous phenomena such as nucleation, aggregation, breakage and evaporation, and due to continuous phenomena such as convection and diffusion. Examples of industrial processes, involving the evolution of a particle population include, but certainly are not limited to, precipitation, polymerization and combustion (Becker et al., 2014), sprays (Laurent and Massot, 2001) and aerosols (McGraw, 1997; McGraw and Wright, 2003).

In this work, we concentrate on the case of a NDF with only one internal coordinate, representing the particle size. Approximate solutions of the corresponding PBE can be determined using several approaches, including Monte-Carlo methods (Lin et al., 2002; Meimaroglou and Kiparissides, 2007; Rosner and Yu, 2001; Smith and Matsoukas, 1998; Zhao et al., 2007; Zhao and Zheng, 2013), which, however, present challenges in practical applications due to their computational cost. Some authors introduce a discretization along

the size variable, leading to the sectional method or the method of classes (Alopaeus et al., 2006; Balakin et al., 2014; Bannari et al., 2008; Becker et al., 2011; Hounslow et al., 1988; Hounslow, 1990; Kumar and Ramkrishna, 1996a,b; Muhr et al., 1996; Puel et al., 2003; Vanni, 2000). Similarly to Monte Carlo methods, this approach is often computationally too demanding when applied to large-scale problems of industrial interest, as observed by Marchisio et al. (2003b). To overcome this issue, hybrid methods between sectional and moment methods are developed (see Nguyen et al. (2016) and references therein), but they are not the subject of this paper.

A widely adopted and sufficiently accurate approach to find approximate solutions of the PBE for engineering applications is the quadrature method of moments (QMOM), originally introduced by McGraw (1997), and extensively applied to several problems in chemical engineering (see Gavi et al. (2007); Marchisio and Fox (2013); Petitti et al. (2010) for examples). The QMOM approach considers a discrete set of moments of the NDF, constituted by an even number of moments. The NDF is then approximated with a discrete weighted sum of Dirac delta functions, uniquely determined by means of a moment inversion algorithm (Gautschi, 2004; Gordon, 1968; Wheeler, 1974). The extended QMOM (EQMOM) (Yuan et al., 2012) introduced the capability of using a basis of non-negative kernel density functions (KDF) to approximate the NDF in place of Dirac delta functions. This development allows some of the limitations of QMOM, that appear when dealing with problems that require the evaluation of the NDF at a particular value of the internal coordinate (i.e. problems involving evaporation term or any other continuous size decreasing term Massot et al. (2010)), to be addressed.

Yuan et al. (2012) proposed the EQMOM procedure for β and Γ KDF, while Madadi-Kandjani and Passalacqua (2015) considered log-normal KDF. The EQMOM reconstruction can be done for every realizable moment set (i.e. moments of a positive NDF), just not reproducing eventually the last moment. In particular, it can deal with the degenerate cases, encountered when the moments are not strictly realizable: the only possible representation of the NDF is then a sum of weighted Dirac delta functions, thus describing a population of particles of only one or a few sizes, as in the case of nucleation. Numerically, this possibility was achieved with the moment inversion algorithm of Nguyen et al. (2016).

In this work we discuss the implementation of the EQMOM approach into the open-source toolbox for computational fluid dynamic (CFD) OpenFOAM® (OpenFOAM, 2015), as part of the OpenQBMM (2016a) project. We limit our attention to a univariate PBE, where the internal coordinate of the NDF is the particle size. We describe the implementation of EQMOM with log-normal KDF as an example, but without loss of generality in the presentation of the computational framework, which was designed to accommodate any KDF defined on the set of positive real numbers $\mathbb{R}^+$. We then discuss the implementation of realizable kinetic fluxes for advection, which guarantee the transported moments are realizable if the step used for time integration satisfies a realizability condition similar to the Courant-Friedrichs-Lewy condition. Particular attention is put in detailing the implementation of the procedure used to determine the approximate NDF, which always ensures that the maximum possible number of moments is conserved (Nguyen et al., 2016). The PBE solver is then verified considering aggregation and breakage

problems studied by Vanni (2000), comparing the predicted results with both the rigorous solution from Vanni (2000) and the numerical solution obtained with EQMOM by Madadi-Kandjani and Passalacqua (2015). Finally, a case involving spatial transport is considered for validation purposes, which consists of an aggregation and breakage problem in a Taylor–Couette reactor. The system was experimentally studied by Serra and Casamitjana (1998a,b); Serra et al. (1997), considering the same test case discussed in Marchisio et al. (2003a). Numerical results obtained with the CFD-PBE solver developed as part of the present work are compared to experiments, showing satisfactory results.

2. The population balance equation

The PBE (Marchisio et al., 2003a; Marchisio and Fox, 2013; Ramkrishna, 2000) accounting for the evolution of a univariate NDF with internal coordinate ξ, representing the particle size, is

$$\frac{\partial n\left(\xi,\mathbf{x},t\right)}{\partial t}+\nabla_{\mathbf{x}}\cdot\left[n\left(\xi,\mathbf{x},t\right)\mathbf{U}\right]-\nabla_{\mathbf{x}}\cdot\left[\Gamma\nabla_{\mathbf{x}}n\left(\xi,\mathbf{x},t\right)\right]+\nabla_{\xi}\cdot\left[G(\xi)n\left(\xi,\mathbf{x},t\right)\right]=\bar{B}^{a}\left(\xi,\mathbf{x},t\right)-\bar{D}^{a}\left(\xi,\mathbf{x},t\right)+\bar{B}^{b}\left(\xi,\mathbf{x},t\right)-\bar{D}^{b}\left(\xi,\mathbf{x},t\right)+\mathcal{N}(\xi,\mathbf{x},t)\quad(1)$$

where $n(\xi,\mathbf{x},t)$ is the NDF, $\mathbf{U}$ is the velocity of the carrier fluid, Γ is the diffusivity, $G(\xi)$ is the growth rate, $\bar{B}\left(\xi,\mathbf{x},t\right)$ and $\bar{D}\left(\xi,\mathbf{x},t\right)$ are, respectively, the rate of change of n due to birth and death, in the aggregation process when the a exponent is present and in the breakage process when a b exponent is present, and $\mathcal{N}(\xi,\mathbf{x},t)$ the rate of change due to nucleation. Let us notice that we assumed the particle size is sufficiently small to have negligible

influence on the carrier fluid. This allows the velocity $\mathbf{U}$ to be assumed equal to the local fluid velocity, and independent of the particle size.

The diffusivity Γ, assumed to be independent from the particle size ξ, is defined as the sum of a laminar and a turbulent contribution: $\Gamma = \Gamma_\mathrm{l} + \Gamma_\mathrm{t}$. The turbulent diffusivity is calculated as the ratio of the turbulent viscosity μ_t and the turbulent Schmidt number σ_t: $\Gamma_\mathrm{t} = \mu_\mathrm{t}/\sigma_\mathrm{t}$.

Following Marchisio and Fox (2013); Marchisio et al. (2003b); Randolph and Larson (1988), the terms describing aggregation and breakage phenomena are written in continuous form as:

$$\bar{B}^a(\xi, \mathbf{x}, t) = \frac{\xi^2}{2}\int_0^\xi \frac{\beta\left(\left(\xi^3-\xi'^3\right)^{1/3}, \xi'\right)}{\left(\xi^3-\xi'^3\right)^{2/3}} n\left(\left(\xi^3-\xi'^3\right)^{1/3}, \mathbf{x}, t\right) n(\xi', \mathbf{x}, t)\,\mathrm{d}\xi', \quad (2)$$

$$\bar{D}^a(\xi, x, t) = n(\xi, \mathbf{x}, t)\int_0^\infty \beta(\xi, \xi')\, n(\xi', \mathbf{x}, t)\, d\xi', \quad (3)$$

$$\bar{B}^b(\xi, \mathbf{x}, t) = \int_\xi^\infty a(\xi')\, b(\xi|\xi')\, n(\xi', \mathbf{x}, t)\,\mathrm{d}\xi', \quad (4)$$

$$\bar{D}^b(\xi, \mathbf{x}, t) = a(\xi)\, n(\xi, \mathbf{x}, t). \quad (5)$$

Growth and nucleation terms were not considered in the example applications presented in this work to verify and validate the implementation of the EQMOM procedure, however they have been implemented in the PBE solver, and their testing is left to future work. These terms and their numerical treatment are kept in the description of the theory presented in this work for completeness and as documentation of the code implementation for the interested reader.

3. The extended quadrature method of moments

The approximate solution of the PBE of Eq. (1) is obtained in this work by solving transport equations for a finite set of the moments of the NDF. In the case of a univariate NDF, the moments are defined as:

$$M_k(t) = \int_0^{+\infty} n\left(\xi, \mathbf{x}, t\right) \xi^k \mathrm{d}\xi. \tag{6}$$

The transport equation for the moment of order k is obtained by multiplying the PBE (Eq. (1)) by ξ^k and integrating over $[0, +\infty[$. Under the previously discussed assumptions on the velocity and the diffusivity, such transport equation is

$$\begin{aligned} \frac{\partial M_k\left(\mathbf{x}, t\right)}{\partial t} + \nabla_{\mathbf{x}} \cdot \left[M_k\left(\mathbf{x}, t\right) \mathbf{U}\right] - \nabla_{\mathbf{x}} \cdot \left[\Gamma \nabla M_k\left(\mathbf{x}, t\right)\right] + \bar{G}_k\left(\mathbf{x}, t\right) \\ = \bar{B}_k^a\left(\mathbf{x}, t\right) - \bar{D}_k^a\left(\mathbf{x}, t\right) + \bar{B}_k^b\left(\mathbf{x}, t\right) - \bar{D}_k^b\left(\mathbf{x}, t\right) + \bar{\mathcal{N}}_k\left(\mathbf{x}, t\right). \end{aligned} \tag{7}$$

The evaluation of the growth, aggregation and breakup terms in Eq. (7) requires the NDF to be known, in addition to the kernel functions a and β. However, because the NDF evolves in space and time, it is not known a priori, and it has to be approximated from the transported moments.

This can be achieved by writing an approximant of the NDF as a weighted sum of non-negative KDF $\delta_\sigma\left(\xi, \xi_\alpha\right)$ (Yuan et al., 2012)

$$n\left(\xi\right) \approx p_{\mathrm{N}}\left(\xi\right) = \sum_{\alpha=1}^{\mathrm{N}} w_\alpha \delta_\sigma\left(\xi, \xi_\alpha\right) \tag{8}$$

where N is the number of KDF used to approximate the NDF, the KDF $\delta_\sigma\left(\xi, \xi_\alpha\right)$ is chosen to formally tend to the Dirac delta function $\delta\left(\xi - \xi_\alpha\right)$ when σ tends to zero, w_α are the non-negative weights of each KDF (*primary* quadrature weights), and ξ_α are the corresponding quadrature abscissae (*primary* abscissae). These parameters $\left(w_\alpha, \xi_\alpha\right)_{\alpha=1,\ldots,\mathrm{N}}$ and σ have to

be computed from $(M_k)_{k=0}^{2N}$ in such a way that this moment set represents the moments of the reconstructed NDF. We use log-normal KDF (Madadi-Kandjani and Passalacqua, 2015) in all the problems considered in this work because the support of the NDF in these problems is $\mathbb{R}^+$:

$$\delta_\sigma(\xi, \mu) = \frac{1}{\xi\sigma\sqrt{2\pi}} \, \mathrm{e}^{-\frac{(\ln \xi - \xi_\alpha)^2}{2\sigma^2}}, \quad \xi, \xi_\alpha, \sigma \in \mathbb{R}^+, \tag{9}$$

however also the Γ KDF discussed in Yuan et al. (2012) is implemented in the OpenQBMM PBE solver. The primary quadrature is determined with the algorithm described in Nguyen et al. (2016), whose implementation is detailed in Sec. 4.4. Once the NDF in Eq. (8) is reconstructed, it is used to calculate integrals that appear in source terms for the moment transport equations, as described in Yuan et al. (2012). To this purpose, a secondary quadrature, with weights $w_{\alpha\beta}$ and abscissae $\xi_{\alpha\beta}$, is determined by considering the recurrence relation that defines the family of orthogonal polynomials with respect to the measure defined from the KDF, and solving the eigenvalue problem associated to the Jacobi matrix defined by this relationship (Gautschi, 2004). In performing this calculation, the Stieltjes-Wigert quadrature is considered for log-normal KDF (Weisstein, 1998; Wilck, 2001), while Laguerre quadrature is used for gamma KDF (Gautschi, 2004). While, in principle, the case of a log-normal KDF could be addressed with a change of variable, allowing Hermite quadrature to be adopted (Madadi-Kandjani and Passalacqua, 2015), it is worth noticing that only the Stieltjes-Wigert quadrature guarantees the correct preservation of the moments of the NDF, and as such it is used in this work.

The term describing molecular growth is given by

$$\bar{G}_k(\mathbf{x},t) = -k\int_0^\infty \xi^{k-1}G(\xi)n(\xi,\mathbf{x},t)\,\mathrm{d}\xi \approx -k\sum_{\alpha=1}^{\mathrm{N}} w_\alpha \sum_{\beta=1}^{\mathrm{N}_\alpha} w_{\alpha\beta}\xi_{\alpha\beta}^{k-1}G(\xi_{\alpha\beta},\mathbf{x},t). \quad (10)$$

The source terms due to birth and death of particles because of aggregation and breakage are

$$\bar{B}_k^a(\mathbf{x},t) = \frac{1}{2}\int_0^\infty n(\xi',\mathbf{x},t)\int_0^\infty \beta(\xi,\xi')\left(\xi^3+\xi'^3\right)^{k/3} n(\xi,\mathbf{x},t)\,\mathrm{d}\xi\mathrm{d}\xi'$$
$$\approx \frac{1}{2}\sum_{\alpha_1=1}^{\mathrm{N}} w_{\alpha_1}\sum_{\beta_1=1}^{\mathrm{N}_\alpha} w_{\alpha_1\beta_1}\sum_{\alpha_2=1}^{\mathrm{N}} w_{\alpha_2}\sum_{\beta_2=1}^{\mathrm{N}_\alpha} w_{\alpha_2\beta_2}\left(\xi_{\alpha_1\beta_1}^3+\xi_{\alpha_2\beta_2}^3\right)^{k/3}\beta_{\alpha_1\beta_1\alpha_2\beta_2} \quad (11)$$

$$\bar{D}_k^a(\mathbf{x},t) = \int_0^\infty \xi^k n(\xi,\mathbf{x},t)\int_0^\infty \beta(\xi,\xi')\,n(\xi',\mathbf{x},t)\,\mathrm{d}\xi'\mathrm{d}\xi \approx \sum_{\alpha_1=1}^{\mathrm{N}} w_{\alpha_1}\sum_{\beta_1=1}^{\mathrm{N}_\alpha} w_{\alpha_1\beta_1}\xi_{\alpha_1\beta_1}^k\sum_{\alpha_2=1}^{\mathrm{N}} w_{\alpha_2}\sum_{\beta_2=1}^{\mathrm{N}_\alpha} w_{\alpha_2\beta_2}\beta_{\alpha_1\beta_1\alpha_2\beta_2} \quad (12)$$

$$\bar{B}_k^b(\mathbf{x},t) = \int_0^\infty \xi^k\int_0^\infty a(\xi')\,b(\xi|\xi')\,n(\xi',\mathbf{x},t)\,\mathrm{d}\xi'\mathrm{d}\xi \approx \sum_{\alpha=1}^{\mathrm{N}} w_\alpha\sum_{\beta=1}^{\mathrm{N}_\alpha} w_{\alpha\beta}a_{\alpha\beta}\bar{b}_{\alpha\beta}^k \quad (13)$$

$$\bar{D}_k^b(\mathbf{x},t) = \int_0^\infty \xi^k a(\xi)\,n(\xi,\mathbf{x},t)\,\mathrm{d}\xi \approx \sum_{\alpha=1}^{\mathrm{N}} w_\alpha\sum_{\beta=1}^{\mathrm{N}_\alpha} w_{\alpha\beta}\xi_{\alpha\beta}^k a_{\alpha\beta}. \quad (14)$$

4. The numerical solution procedure

The transport equations for the moments (Eq. (7)) are discretized using a finite-volume procedure (Ferziger and Peric, 2002; LeVeque, 2002), with kinetic-based spatial fluxes (Desjardins et al., 2008; Perthame, 1990) to ensure moment realizability.

4.1. Spatial fluxes

The discretization of the moment advection term is key to ensure moment realizability, and achieve a robust solution procedure. The problem of moment realizability caused by convection schemes is well known in the literature (Desjardins et al., 2008; Wright, 2007), and it appears when using conventional numerical schemes of order higher than one, since the application of limiters to the individual transported moments is not a sufficient condition to ensure the realizability of the transported moment set. Vikas et al. (2011, 2013) proposed to implement kinetic schemes (Perthame, 1990) where the convection flux for each moment is computed from the quadrature approximation of the transported moment set. In these schemes, the high-order reconstruction is applied only to the quadrature weights, while the reconstructed quadrature abscissae are constant in the cell, hence the name of quasi high-order schemes. This approach allows the realizability of the moment set to be preserved if a constraint on the time-step size is satisfied. This realizability constraint becomes the Courant-Friedrichs-Lewy (CFL) condition, if weights and abscissae are reconstructed on cell faces with a first-order scheme, which, therefore, always ensures moment realizability if the CFL condition is satisfied.

The numerical scheme used to compute face values of a variable in OpenFOAM can be selected independently for any variable, or specifying the scheme as argument of the `fvc::interpolate` function provided by the OpenFOAM framework. As a consequence, the details of the implementation of high-order reconstruction schemes are not discussed here, and our description is limited to the general structure of kinetic-based schemes for

quadrature-based moment methods.

We assume the flow velocity vector $\mathbf{U}$ is known at cell centers. We indicate with $\mathbf{U}_{\text{own}}$ and $\mathbf{U}_{\text{nei}}$ the interpolated face values of such velocity on the owner and neighbour side of the cell face, respectively. Similarly, we indicate with $M_{k,\text{own}}$ and $M_{k,\text{nei}}$ the moments computed on the owner and neighbour side of the cell face (see Fig. 1), defined as

$$M_{k,\text{own}} = \sum_{\alpha=1}^{\text{N}_\text{f}} w_{\alpha,\text{own}} \xi_{\alpha,\text{own}}^k, \; M_{k,\text{nei}} = \sum_{\alpha=1}^{\text{N}_\text{f}} w_{\alpha,\text{own}} \xi_{\alpha,\text{nei}}^k, \tag{15}$$

where N_f is the number of quadrature nodes used to define the quadrature approximation of the NDF used to compute the spatial fluxes, $w_{\alpha,\text{own}}$ and $w_{\alpha,\text{nei}}$ are the face, and $\xi_{\alpha,\text{own}}$, $\xi_{\alpha,\text{nei}}$ the face values of the quadrature abscissae. Following Laurent and Nguyen (2016), the spatial fluxes are calculated as a function of a different quadrature approximation with respect to the one determined with the EQMOM procedure. If an odd number of moments is realizable, this quadrature approximation is obtained using a $N + 1$ point Gauss-Radau quadrature formula, which allows the $2\text{N} + 1$ moments to be preserved, with one quadrature abscissa set to zero. However, if the number of realizable moments is even, the regular Gauss quadrature is used to define the face flux. This approach is independent from the reconstruction of the NDF, and allows the fluxes to be defined without relying on the secondary quadrature approximation, leading to a more robust formulation of the numerical scheme, with the additional benefit of a slightly lower computational cost due to the reduced number of terms involved in the summations in Eq. 16 compared to EQMOM. Details on the rationale of the definition of the advection schemes for moment methods are provided in Laurent and Nguyen

(2016), where high-order schemes for moment methods are also developed. The convective flux of the moment M_k is then found computing

$$\varphi_{M_k} = M_{k,\text{nei}} \min(\mathbf{U}_{\text{nei}} \cdot \mathbf{n}, 0) + M_{k,\text{own}} \max(\mathbf{U}_{\text{own}} \cdot \mathbf{n}, 0), \tag{16}$$

and finding the rate of change of the moment M_k by integrating φ_{M_k} over the cell faces.

4.2. Diffusion term

The discretization of diffusion term in the moment transport equations does not present particular problems when a traditional second-order scheme (Ferziger and Peric, 2002) is used, as explained in Vikas et al. (2013). As a consequence, no special treatment is adopted to ensure moment realizability when the diffusion term is discretized, because second-order accuracy is considered sufficient for most practical applications. The diffusion term in the moment transport equations is therefore discretized with the `fvm::laplacian(gamma, Mk)` operator provided by OpenFOAM, where `gamma` is the diffusivity and `Mk` is the moment of order k. It is worth observing that this approach suffices for size-independent diffusion, however, if size-dependent diffusion needs to be considered, the diffusion term will have to be computed as a function of the quadrature approximation, and treated as an explicit source term in the transport equations for the moments, as discussed in Vikas et al. (2013).

4.3. Source terms

The source terms for aggregation, breakage and nucleation are introduced as explicit source terms in the moment transport equations, using the standard mechanism available in OpenFOAM. Moreover, to ensure realizability,

explicit Euler methods with small enough time steps can be used, as well as any convex combination of Euler explicit time steps (Nguyen et al., 2016), such as the strong-stability-preserving (SSP) explicit Runge-Kutta methods (Gottlieb et al., 2011), which are high-order ODE solvers. An example of multi-step adaptive scheme that takes advantage of this property is described and demonstrated in Nguyen et al. (2016).

4.4. Moment inversion

A key aspect of the numerical solution procedure is the moment inversion to find the primary quadrature weights w_α, abscissae ξ_α and the parameter σ of the KDF, in such a way that the moments of the reconstruction defined by Eq. (8) are the considered moment set. The approach implemented in the OpenQBMM-PBE solver is based on the work of Nguyen et al. (2016), which represents an improvement of the method proposed in Yuan et al. (2012) and also used in Madadi-Kandjani and Passalacqua (2015). The key difference between the method in Yuan et al. (2012) and the new one proposed in Nguyen et al. (2016) consists in an efficient procedure to check the strict realizability of the moment set, and the conservation of the largest possible subset of transported moments, which is not always achieved using the approach of Yuan et al. (2012).

The algorithm is based on the possibility to use an efficient quadrature algorithm based, for example, on the Wheeler (1974) algorithm. Introducing the variables $M_k^* = \sum_{\alpha=1}^{\mathrm{N}} w_\alpha \xi_\alpha^k$, the KDF is chosen in such a way that, for a fixed value of σ, there exists a linear relation between the moments $\mathbf{M}_K = (M_0, \ldots, M_K)$ of the reconstruction and $\mathbf{M}_K^* = (M_0^*, \ldots, M_K^*)$:

$\mathbf{M}_K = A_K(\sigma)\mathbf{M}_K^*$. For a log-normal KDF, it is given by

$$M_k^* = M_k \, \mathrm{e}^{-k^2\sigma^2/2}, \tag{17}$$

in such a way that the matrix $A_K(\sigma)$ is diagonal. Then, from the transported moment vector $\mathbf{M}_{2\mathrm{N}} = (M_0, \ldots, M_{2\mathrm{N}})$, one can define the function $\bar{M}_{2\mathrm{N}}(\sigma)$ in the following way: if $\mathbf{M}_{2\mathrm{N}-1}^*(\sigma) = A_{2\mathrm{N}-1}(\sigma)^{-1}\mathbf{M}_{2\mathrm{N}-1}$ is strictly realizable, which corresponds to $\sigma < \sigma_{\mathrm{max},2\mathrm{N}}$, then one computes the corresponding quadrature weights and abscissae $(w_\alpha(\sigma), \xi_\alpha(\sigma))_{\alpha=1,\ldots,\mathrm{N}}$ and $M_{2\mathrm{N}}(\sigma)$ is the moment of order 2N of the reconstructed NDF defined by Eq. (8) with the parameters σ and $(w_\alpha(\sigma), \xi_\alpha(\sigma))_{\alpha=1,\ldots,\mathrm{N}}$. When $\sigma \geq \sigma_{\mathrm{max},2\mathrm{N}}$, the function $\bar{M}_{2\mathrm{N}}(\sigma)$ is set to a large value[2] L. For a log-normal KDF, this function is given by

$$\bar{M}_{2\mathrm{N}}(\sigma) = \begin{cases} \sum_{\alpha=1}^{\mathrm{N}} w_\alpha(\sigma)\xi_\alpha(\sigma)^{2\mathrm{N}} z^{(2\mathrm{N})^2} & \sigma < \sigma_{\mathrm{max},2\mathrm{N}} \\ L & \sigma \geq \sigma_{\mathrm{max},2\mathrm{N}}, \end{cases} \tag{18}$$

where $z = \mathrm{e}^{\sigma^2/2}$. This helper function is used to define the target function $J_{2\mathrm{N}}$, whose roots are the values of the parameter σ we seek, with

$$J_{2\mathrm{N}}(\sigma) = \frac{M_{2\mathrm{N}} - \bar{M}_{2\mathrm{N}}(\sigma)}{M_{2\mathrm{N}}}. \tag{19}$$

If Eq. 19 has no root, then the last moment will not be reproduced by the reconstructed NDF. One then will have to minimize the error on it, by an optimal choice of σ. In any case, at least all moments of orders 0 to $2\mathrm{N} - 1$ will be well reproduced by the reconstruction.

[2] A value of 1.0×10^{16} was used in the implementation, which corresponds to the definition of the GREAT constant in OpenFOAM.

It can happen that the transported moment vector $\mathbf{M}_{2\mathrm{N}}$ is not strictly realizable (degenerate case), when it corresponds to a NDF that is necessarily a sum of a few weighted Dirac delta functions. This is the case for example, in problems involving nucleation, and at the beginning of aggregation processes. Only one representation is then possible and the moment inversion has to be adapted in this case. The first step of the moment inversion procedure is then to study the realizability of the moment vector. Differently from what done in Madadi-Kandjani and Passalacqua (2015); Yuan et al. (2012), which directly evaluated the Hankel determinants associated with the set of transported moments, this is achieved computing the values of the ζ_k quantities defined as in Dette and Studden (1997), which allow the size $\mathrm{N_r} \leq 2\mathrm{N}+1$ of the largest subset of strictly realizable moments $\mathbf{M}_{\mathrm{N_r}-1}$ to be found. This approach is more computationally efficient than evaluating the Hankel determinants directly, as briefly discussed later, and explained in detail in Nguyen et al. (2016). The quantities ζ_k are directly related to the Hankel determinants

$$\underline{H}_{2k} = \begin{vmatrix} M_0 & \dots & M_k \\ \vdots & & \vdots \\ M_k & \dots & M_{2k} \end{vmatrix}, \quad \underline{H}_{2k+1} = \begin{vmatrix} M_1 & \dots & M_{k+1} \\ \vdots & & \vdots \\ M_{k+1} & \dots & M_{2k+1} \end{vmatrix}, \tag{20}$$

as follows[3]

$$\zeta_k = \frac{\underline{H}_{k+1}\underline{H}_{k-2}}{\underline{H}_k\underline{H}_{k-1}}, \; k = 0, 1 \dots, \tag{21}$$

with $\underline{H}_{-2} = \underline{H}_{-1} = \underline{H}_0 = 1$. They are also related to the coefficients of the

[3]Note that ζ_k is here re-defined to start the numbering from zero rather than from one, for consistency with the implementation.

recurrence relation that defines the family of orthogonal polynomials $(P_k)_{k\geq 0}$ with respect to a measure associated to the moments:

$$P_{k+1}(X) = (X - a_k)P_k(X) - b_k P_{k-1}(X), \tag{22}$$

with $a_0 = \zeta_1$ and for $k \geq 1$: $b_k = \zeta_{2k-1}\zeta_{2k}$ and $a_k = \zeta_{2k}+\zeta_{2k+1}$. Thanks to this relation, the values of ζ_k are computed using the Q-D algorithm described in Dette and Studden (1997), or, more effectively, with a modified version of the Chebyshev algorithm (Wheeler, 1974) to include the calculation of ζ_k (Nguyen et al., 2016). Following Dette and Studden (1997), the positivity of ζ_k ensures the strict realizability of the moment set. Based on the largest value of k for which $\zeta_k > 0$, it is then possible to identify the subset of strictly realizable moments in the transported moment set.

Depending on the value of strictly realizable moments $\mathrm{N_r}$, the following cases are possible:

1. If $\mathrm{N_r} < 2$, the procedure terminates because the number of strictly realizable moments is insufficient to define a quadrature formula.
2. If $\mathrm{N_r}$ is an even integer, the Wheeler (1974) algorithm is applied to $\mathbf{M}_{\mathrm{N_r}}$, and $\mathrm{N_r}/2$ primary quadrature weights and abscissae are calculated. In this case, the parameter σ is set to zero, and no attempt is made to reconstruct a continuum distribution because the direct application of the standard QMOM procedure, relying on Dirac delta functions, ensures the conservation of the $\mathrm{N_r}$ strictly realizable moments.
3. If $\mathrm{N_r}$ is an odd integer, the complete EQMOM procedure is applied to the $\mathrm{N_r}$ first $\mathrm{N_r}-1$ moments, i.e. from $\mathbf{M}_{\mathrm{N_r}-1}$. This allows to determine the $(\mathrm{N_r}-1)/2$ primary quadrature weights and abscissas, the parameter

σ, and the secondary quadrature. The objective of the procedure is to determine the value of $\sigma \in \mathbb{R}^+$ as a root of the non-linear function $J_{\mathrm{N_r}-1}$ thus ensuring the conservation of the entire $\mathbf{M}_{\mathrm{N_r}-1}$, when it exists, or to minimize the error on the last moment of the set, whenever a value of σ that guarantees its exact conservation cannot be found. The procedure is iterative, and operates as follows:

(a) An initial interval where to search for the value of σ is determined considering the value of the σ parameter that ensures that $\mathbf{M}_3^*(\sigma)$ is strictly realizable. We will indicate this value of σ as $\sigma_{\max,4}$, and consider $I_0 =]0, \sigma_{\max,4}[$ as initial interval. For a log-normal KDF, we have

$$\sigma_{\max,4} = \min\left(\sqrt{2\log\frac{\sqrt{M_0 M_2}}{M_1}}, \sqrt{2\log\frac{\sqrt{M_1 M_3}}{M_2}}\right) \tag{23}$$

It is important to observe, however, that $\sigma_{\max,4}$ is not a valid value for the σ parameter, because the condition on the strict realizability of $\mathbf{M}_k^*(\sigma)$ for $k \geq 4$ would further reduce the right bound of the interval of σ. This however does not represent a problem in our procedure, since the interval we determine is only used to initially start the search for σ.

(b) The function described in Eq. (19) changes sign in I_0 by construction, as a consequence of the definition of $\bar{M}_{2\mathrm{N}}(\sigma)$ in Eq. (18). We then apply Ridder's algorithm (Ridders, 1979) to the function $J_{\mathrm{N_r}-1}(\sigma)$ to find a root for the target function. If this root represents an actual solution that allows the moment set to be preserved, then the value of σ found from Ridder's algorithm will

be used. If the computed value of σ does not preserve the moment set, a minimization procedure based on the golden search algorithm (Press et al., 2007) is applied to $J_{\mathrm{N_r}-1}(\sigma)^2$, in order to find the value of σ which minimizes the distance of $J_{\mathrm{N_r}-1}(\sigma)$ from zero.

(c) Once the value of the parameter σ is determined, the secondary quadrature weights and abscissae are computed by means of the standard eigenvalue problem used to calculate the roots of polynomials orthogonal to the chosen KDF (Gautschi, 2004).

The steps of the EQMOM inversion algorithm are schematically represented in Fig. 2.

5. Code structure

The solution procedure for univariate PBE was implemented into OpenFOAM creating a general data and implementation structure which allow the extension to multivariate problems, and the straightforward addition of sub-models such as kernels describing new physics. Additionally, the functionality of OpenFOAM was leveraged to couple the implementation of the PBE solver with fluid solvers, re-using the existing thermal and turbulence models. In the following subsections we provide a brief description of the code structures and implementation choices made during the development of OpenQBMM-PBE.

5.1. Basic moment inversion

We call basic moment inversion the process of calculating N quadrature weights and abscissae from a moment vector of dimension 2N. This pro-

cess is achieved by means of the algorithm proposed by Wheeler (1974).
A specific C++ object, called `univariateMomentSet`, was derived for the uni-dimensional array of scalars object `scalarDiagonalMatrix` provided by the OpenFOAM library. The `univariateMomentSet` object combines the use of ζ_k to verify the strict realizability of the moment set, with the Wheeler (1974) algorithm to perform the moment inversion. The procedure is schematically represented in Fig. 3. For each moment set that has to be inverted, the maximum even number of strictly realizable moments, which we call number of invertible moments[4] $\mathrm{N_I}$, is determined by checking the positivity of ζ_k and taking the largest even integer smaller than the number of strictly realizable moments $\mathrm{N_r}$. Once $\mathrm{N_I}$ is found, the procedure verifies that $\mathrm{N_I} \geq 2$, which is required to perform the inversion. If this condition is satisfied, the Jacobi matrix (see Appendix A) is constructed and the associated eigenvalue problem is solved to determine quadrature weights and abscissae.

5.2. Extended moment inversion

The extended moment inversion procedure is implemented in a general form, in order to accommodate different types of KDF with support on $\mathbb{R}^+$. The type of KDF can be selected by the user at run-time as conventionally done in OpenFOAM for model selection, by means of a keyword in an input file.
A base class named `extendedMomentInversion` implements the algorithm to find the value of the parameter σ, and the general parts of the procedure to define the secondary quadrature (Fig. 2). Specialized classes derived from

[4]The number of invertible moments coincides with the number of strictly realizable moments, if this is even, and it is equal to $\mathrm{N_r} - 1$, if the $\mathrm{N_r}$ is odd.

`extendedMomentInversion` implement the part of the algorithm specific to a KDF such as the expression of the KDF itself, the relationship between M_k and M_k^*, and the upper extremum $\sigma_{\max}$ of the interval I_0.

5.3. Population balance solver

The PBE is solved in a separate class, which also uses the run-time selection mechanism, allowing future extensions to multivariate problems to be implemented. A base class called `populationBalanceModel` implements the generic structure required for run-time selection of the type of PBE to be solved. The actual implementation of the PBE solver is contained in the derived class `univariatePopulationBalance`, which provides methods to calculate the convection, diffusion and source terms for the specific PBE.

6. Verification of the PBE solver

The PBE solver was verified considering a set of zero-dimensional problems involving aggregation and breakage (Vanni, 2000). The solutions obtained in these cases were compared to the numerical solution obtained with a MATLAB code implementing EQMOM in Madadi-Kandjani and Passalacqua (2015), which relied on the solution approach detailed in Yuan et al. (2012) extended to log-normal KDF, and to the rigorous solution of the same problems reported by Vanni (2000).

In this situation, Eq. (1) reduces to Eq. (24), where only the source terms due to aggregation and breakup remain, while diffusion and advection are not considered:

$$\frac{\partial n\left(\xi,\mathbf{x},t\right)}{\partial t} = \bar{B}^a\left(\xi,\mathbf{x},t\right) - \bar{D}^a\left(\xi,\mathbf{x},t\right) + \bar{B}^b\left(\xi,\mathbf{x},t\right) - \bar{D}^b\left(\xi,\mathbf{x},t\right). \quad (24)$$

The cases considered in this validation study are reported in Tab. 1, and correspond to those examined in Madadi-Kandjani and Passalacqua (2015). The table also indicates the number of primary and secondary quadrature nodes used in each case. The aggregation and breakage kernels used in the study are reported in Tab. 2 and 3, respectively. The expressions for the daughter distribution that appear in the breakage kernel are summarized in Tab. 4.

The simulation results shown in Figs. 4–8 show the time evolution of the value of M_0 and of the average particle size $\mathrm{d}_{43} = M_4/M_3$. The agreement between the numerical solution obtained with MATLAB (Madadi-Kandjani and Passalacqua, 2015), and the one obtained with the OpenFOAM implementation of the EQMOM procedure is excellent: in all the cases under examination, the two solutions match. This comparison serves as verification of the EQMOM procedure implemented into OpenFOAM. The comparison to the rigorous solution of Vanni (2000) shows good agreement in all the cases under consideration, with the exception of case 3 (Fig. 6), in which some deviation of the numerical solution from the rigorous solution can be observed for $t \in [1, 4]$ s.

7. Validation of CFD-PBE solver

The solution of the full PBE with an inhomogeneous velocity field is tested and validated using the case studied by Marchisio et al. (2003a) in a Taylor–Couette reactor made by two concentrical cylinders with diameter $D_1 = 193$ mm, and $D_2 = 160$ mm. The height of the system is $H = 360$ mm.

7.1. Kernels for the PBE

The aggregation kernel used in this case is given by the sum of the kernel for Brownian motion (Eq. (25)) (Smoluchowski, 1917), combined with the kernel proposed by Adachi et al. (1994) for particles whose size is smaller than the local Kolomogorov microscale (Eq. (26)):

$$\beta(\xi, \xi') = \frac{2k_{\mathrm{B}}}{3\mu} \frac{(\xi + \xi')^2}{\xi\xi'} \tag{25}$$

$$\beta(\xi, \xi') = \frac{4}{3}\sqrt{\frac{3\pi\varepsilon}{10\nu}} \left(\xi + \xi'\right)^3 . \tag{26}$$

The breakage kernel of Luo and Svendsen (1996), which depends on the kinematic viscosity ν, the turbulent dissipation rate ε and the particle size ξ, was used:

$$a(\xi) = c_{\mathrm{Br}} \nu^p \varepsilon^q \xi^r . \tag{27}$$

Following Marchisio et al. (2003a), we set $p = 3/4$, $q = -5/4$ and $r = 1$, and we adopt the symmetric fragmentation daughter distribution function (Tab. 4). The coefficient c_{Br} was set equal to 6.0×10^{-4} (Marchisio et al., 2003a).

7.2. Case setup

The Taylor–Couette reactor was modeled assuming symmetry, reducing the computational domain to a rectangular region whose width is $(D_1 - D_2)/2 = 16.5$ mm, and its height is $H = 180$ mm, as schematized in Fig 9. This domain was discretized using 18 cells in the horizontal direction, and 180 in the vertical direction (Marchisio et al., 2003a), leading to a total of 3240 computational cells. The initial particle size distribution is assumed to be a Dirac delta function (uniform size), with a mean particle volume fraction

$\alpha_{\mathrm{p}} = 2.5 \times 10^{-5}$, and an initial particle size $\xi_0 = 2$ μm (Marchisio et al., 2003a). The first five moments of the NDF are considered and, as a consequence, N = 2 primary quadrature nodes are used. The number of secondary quadrature nodes was set equal to $\mathrm{N}_\alpha = 10$. It is worth observing that the initial condition leads to a quadrature representation with only one quadrature node, and null value of the σ parameter. Therefore, the moment inversion procedure will use the standard Wheeler (1974) algorithm to perform the inversion. However, the EQMOM procedure is used as soon as the particle size distribution is not a Dirac delta anymore, and some variance in the particle size appears. The transition between the two algorithms is managed automatically, based on the realizability of the moment set and of the number of moments required to define the quadrature representation of the NDF.

Marchisio et al. (2003a) considered four rotational speeds (75, 125, 165 and 211 RPM), however we limit our study to two rotational speeds for brevity, since the purpose of our investigation is to verify the robustness and accuracy of the computational framework. We consider then $\omega_1 = 75$ RPM, and $\omega_2 = 165$ RPM.

7.3. Results and discussion

The velocity field of the fluid phase in the Taylor–Couette reactor is reported in Fig. 10 for the two cases considered in this work. The volume-averaged turbulent dissipation rate calculated when the flow inside the Taylor–Couette reactor reached steady state is 0.012 m^2/s^3 for the case with rotational speed of 75 RPM, and of 0.147 m^2/s^3 for the case with rotational speed of 165 RPM. These values are consistent with those reported by Marchisio et al. (2003a).

The evolution in time of the normalized mean particle diameter $d = d_{43}/\xi_0$ predicted by the simulations is compared to the experimental data of Serra and Casamitjana (1998a,b); Serra et al. (1997) as reported in Fig. 11. The same value of the coefficient $c_{Br} = 6.0 \times 10^{-4}$, found to give the best match with experimental results by Marchisio et al. (2003a), was used for all the simulations.

Fig. 11(a) shows that the numerical simulation provides a good estimate of the steady-state value of d_{43} for the case with rotational speed of 75 RPM, which is underpredicted by the results obtained with the standard QMOM procedure in Marchisio et al. (2003a). Both the EQMOM and the QMOM approach predict the particle diameter reaches its steady-state value significantly earlier ($t \approx 2000$ s) than what observed in the experiments ($t \approx 12000$ s).

The EQMOM simulation slightly over-predicts the steady-state value of the mean normalized particle diameter (≈ 11) compared to the experimental results (≈ 10) in the case with rotational speed of 165 RPM. The steady state value of the particle size is reached after about 1000 s from the beginning of the simulation, however experimental data show that a slower evolution of the value of d_{43}, with a time required to reach steady state of about 2000 s.

8. Conclusions

The EQMOM was implemented into OpenFOAM to solve univariate population balance equations. The implementation was successfully verified against the numerical results of Madadi-Kandjani and Passalacqua (2015) involving aggregation and breakage problems in a homogoeneous system. The results

were validated against the rigorous solutions obtained by Vanni (2000). The PBE solver was then coupled to a CFD solver to enable the solution of the PBE for inhomogeneous systems with transport of particles due to the fluid motion. This was achieved by implementing kinetic-based fluxes for the moment transport equations. The implementation was validated by simulating shear-driven aggregation and breakage in the Taylor–Couette reactor considered by Marchisio et al. (2003a). Satisfactory results were shown concerning the prediction of the steady-state value of the mean particle diameter.

9. Code repository

The source code of the OpenQBMM-PBE software can be downloaded from the git repository `https://github.com/OpenQBMM`, and is distributed under the terms of the GNU General Public License version 3. The specific version of the code, and the tutorials used to produce the results reported in this work is OpenQBMM 2.0.0 (OpenQBMM, 2016b). The repository also contains all the test cases mentioned in this article, and the corresponding validation data.

10. Acknowledgments

The authors would like to gratefully acknowledge the support of the US National Science Foundation under the SI^2–SSE award NSF–ACI 1440443 and the support of the French National Research Agency (ANR) under grant ANR-13-TDMO-02 ASMAPE for the ASMAPE project.

Appendix A. Inversion algorithm

We briefly summarize here the moment inversion algorithm, based on the work of Wheeler (1974), to perform the moment inversion using the same notation adopted in the implementation. We assume the number of invertible moments is $\mathrm{N_I}$. Let us denote with a_i and b_i, $i \in \{0, 1, \ldots, \mathrm{N_I}/2\}$ the coefficients of the recurrence relation that define the family of orthogonal polynomials with respect to a measure associated to the moments. We also introduce the matrix $S \in \mathbb{R}^{2\mathrm{N_I}+1, 2\mathrm{N_I}+1}$, which is defined as follows in the code:

$$
\begin{aligned}
& a_0 = \frac{M_1}{M_0} \\
& b_0 = 0 \\
& S_{1,i} = M_{i-1},\ i = 1, \ldots, \mathrm{N_I}, \\
& k = 2, \ldots, \mathrm{N_I}/2 + 1, l = k, \ldots, \mathrm{N_I} - k + 2, \\
& S_{k,l} = S_{k-1,l+1} - a_{k-2} S_{k-1,l} - b_{k-2} S_{k-2,l}, \\
& a_{k-1} = \frac{S_{k,k+1}}{S_{k,k}} - \frac{S_{k-1,k}}{S_{k-1,k-1}}, \\
& b_{k-1} = \frac{S_{k,k}}{S_{k-1,k-1}},
\end{aligned}
\tag{A.1}
$$

The matrix $z \in \mathbb{R}^{\mathrm{N_I}/2, \mathrm{N_I}/2}$ is then defined as

$$
\begin{aligned}
& z_{i,i} = a_i,\ i = 0, \ldots, \mathrm{N_I}/2 - 1, \\
& z_{i,i+1} = \sqrt{b_{i+1}},\ i = 0, \ldots, \mathrm{N_I}/2 - 2, \\
& z_{i+1,i} = z_{i,i+1},\ i = 0, \ldots, \mathrm{N_I}/2 - 1
\end{aligned}
\tag{A.2}
$$

Quadrature weights and abscissae are then found as

$$
\begin{aligned}
& w_i = M_0 v_{z,1,i}^2, \\
& \xi_i = \lambda_{z,i},
\end{aligned}
\tag{A.3}
$$

where $\lambda_{z,i}$ is the i-th eigenvalue of z and $v_{x,1,i}$ is the first component of the corresponding eigenvector.

References

Adachi, Y., Stuart, M. A. C., Fokkink, R., Jul. 1994. Kinetics of turbulent coagulation studied by means of end-over-end rotation. Journal of Colloid and Interface Science 165 (2), 310–317.

Alopaeus, V., Laakkonen, M., Aittamaa, J., Oct. 2006. Solution of population balances with breakage and agglomeration by high-order moment-conserving method of classes. Chemical Engineering Science 61 (20), 6732–6752.

Balakin, B. V., Hoffmann, A. C., Kosinski, P., 2014. Coupling STAR-CD with a population-balance technique based on the classes method. Powder Technology 257, 47–54.

Bannari, R., Kerdouss, F., Selma, B., Bannari, A., Proulx, P., 2008. Three-dimensional mathematical modeling of dispersed two-phase flow using class method of population balance in bubble columns. Computers & Chemical Engineering 32 (12), 3224–3237.

Becker, P. J., Puel, F., Dubbelboer, A., Janssen, J., Sheibat-Othman, N., Sep. 2014. Coupled population balance–CFD simulation of droplet breakup in a high pressure homogenizer. Computers & Chemical Engineering 68, 140–150.

Becker, P. J., Puel, F., Henry, R., Sheibat-Othman, N., 2011. Investigation of discrete population balance models and breakage kernels for dilute emulsification systems. Industrial & Engineering Chemistry Research 50 (19), 11358–11374.

Desjardins, O., Fox, R., Villedieu, P., 2008. A quadrature-based moment method for dilute fluid-particle flows. Journal of Computational Physics 227 (4), 2514–2539.

Dette, H., Studden, W. J., 1997. The Theory of Canonical Moments with Applications in Statistics, Probability and Analysis. John Wiley & Sons.

Ferziger, J. H., Peric, M., 2002. Computational Methods for Fluid Dynamics. Springer.

Gautschi, W., 2004. Orthogonal Polynomials: Computation and Approximation. Oxford University Press.

Gavi, E., Rivautella, L., Marchisio, D. L., Vanni, M., Barresi, A. A., Baldi, G., 2007. CFD modelling of nano-particle precipitation in confined impinging jet reactors. Chemical Engineering Research and Design 85 (5), 735–744.

Gordon, R. G., 1968. Error bounds in equilibrium statistical mechanics. Journal of Mathematical Physics 9, 655–662.

Gottlieb, S., Ketcheson, D., Shu, C.-W., 2011. Strong Stability Preserving Runge-Kutta and Multistep Time Discretizations. World Scientific.

Hounslow, M., Ryall, R., Marshall, V., 1988. Discretized population balance for nucleation, growth, and aggregation. AIChE Journal 34 (11), 1821–1832.

Hounslow, M. J., 1990. A discretized population balance for continuous systems at steady state. AIChE Journal 36 (1), 106–116.

Kumar, S., Ramkrishna, D., Apr. 1996a. On the solution of population balance equations by discretization – I. A fixed pivot technique. Chemical Engineering Science 51 (8), 1311–1332.

Kumar, S., Ramkrishna, D., Apr. 1996b. On the solution of population balance equations by discretization – II. A moving pivot technique. Chemical Engineering Science 51 (8), 1333–1342.

Laurent, F., Massot, M., 2001. Multi-fluid Modeling of Laminar Polydispersed Spray Flames: Origin, Assumptions and Comparison of the Sectional and Sampling Methods. Combustion Theory and Modelling 5 (4), 537–572.

Laurent, F., Nguyen, T. T., 2016. Realizable high-order finite-volume schemes for the advection of moment sets of the particle size distribution, submitted.
URL https://hal.archives-ouvertes.fr/hal-01345689

LeVeque, R. J., 2002. Finite Volume Methods for Hyperbolic Problems, 1st Edition. Cambridge University Press.

Lin, Y., Lee, K., Matsoukas, T., 2002. Solution of the population balance

equation using constant–number Monte Carlo. Chemical Engineering Science 57 (12), 2241–2252.

Luo, H., Svendsen, H. F., May 1996. Theoretical model for drop and bubble breakup in turbulent dispersions. AIChE Journal 42 (5), 1225–1233.

Madadi-Kandjani, E., Passalacqua, A., Jul. 2015. An extended quadrature-based moment method with log-normal kernel density functions. Chemical Engineering Science 131, 323–339.

Marchisio, D., Dennis Vigil, R., O. Fox, R., Aug. 2003a. Implementation of the quadrature method of moments in CFD codes for aggregation–breakage problems. Chemical Engineering Science 58 (15), 3337–3351.

Marchisio, D. L., Fox, R. O., 2013. Computational Models for Polydisperse Particulate and Multiphase Systems. Cambridge University Press.

Marchisio, D. L., Vigil, R., Fox, R. O., 2003b. Quadrature method of moments for aggregation-breakage processes. Journal of Colloid and Interface Science 258 (2), 322–334.

Massot, M., Laurent, F., Kah, D., de Chaisemartin, S., 2010. A robust moment method for evaluation of the disappearance rate of evaporating sprays. SIAM Journal on Applied Mathematics 70 (8), 3203–3234.

McGraw, R., 1997. Description of aerosol dynamics by the quadrature method of moments. Aerosol Science and Technology 27 (2), 255–265.

McGraw, R., Wright, D. L., 2003. Chemically resolved aerosol dynamics

for internal mixtures by the quadrature method of moments. Journal of Aerosol Science 34 (2), 189–209.

Meimaroglou, D., Kiparissides, C., 2007. Monte Carlo simulation for the solution of the bi-variate dynamic population balance equation in batch particulate systems. Chemical Engineering Science 62 (1820), 5295–5299.

Muhr, H., David, R., Villermaux, J., Jezequel, P. H., 1996. Crystallization and precipitation engineering-VI. Solving population balance in the case of the precipitation of silver bromide crystals with high primary nucleation rates by using the first order upwind differentiation. Chemical Engineering Science 51 (2), 309–319.

Nguyen, T. T., Laurent, F., Fox, R. O., Massot, M., 2016. Journal of Computational Physics 325, 129–156.

OpenFOAM, 2015. OpenFOAM User Guide. The OpenFOAM Foundation.
URL `www.openfoam.org`

OpenQBMM, 2016a. An open-source implementation of quadrature-based moment methods.
URL `www.openqbmm.org`

OpenQBMM, 2016b. OpenQBMM 2.0.0 Stable for OpenFOAM 4.x. DOI: 10.5281/zenodo.161617.
URL `https://github.com/OpenQBMM/OpenQBMM/releases/tag/OpenQBMM_2.0.0_stable`

Perthame, B., 1990. Boltzmann type schemes for compressible Euler equations in one and two space dimensions. SIAM Journal of Numerical Analysis 29 (1), 1–19.

Petitti, M., Nasuti, A., Marchisio, D. L., Vanni, M., Baldi, G., Mancini, N., Podenzani, F., 2010. Bubble size distribution modeling in stirred gas-liquid reactors with QMOM augmented by a new correction algorithm. AIChE Journal 56 (1), 36–53.

Press, W. H., Teukolsky, S. H., Vetterling, W. T., Flannery, B. P., 2007. Numerical Recipes: The Art of Scientific Computing. Cambridge University Press.

Puel, F., Fvotte, G., Klein, J. P., 2003. Simulation and analysis of industrial crystallization processes through multidimensional population balance equations. part 1: a resolution algorithm based on the method of classes. Chemical Engineering Science 58 (16), 3715–3727.

Ramkrishna, D., 2000. Population Balances: Theory and Applications to Particulate Systems in Engineering. Academic Press, San Diego, CA.

Randolph, A. D., Larson, M. A., 1988. Theory of Particulate Processes: Analysis and Techniques of Continuous Crystallization. Academic Press.

Ridders, C., Nov. 1979. A new algorithm for computing a single root of a real continuous function. IEEE Transactions on Circuits and Systems 26 (11), 979–980.

Rosner, D. E., Yu, S., 2001. MC simulation of aerosol aggregation and simultaneous spheroidization. AIChE Journal 47 (3), 545–561.

Serra, T., Casamitjana, X., Aug. 1998a. Effect of the shear and volume fraction on the aggregation and breakup of particles. AIChE Journal 44 (8), 1724–1730.

Serra, T., Casamitjana, X., Oct. 1998b. Structure of the aggregates during the process of aggregation and breakup under a shear flow. Journal of Colloid and Interface Science 206 (2), 505–511.

Serra, T., Colomer, J., Casamitjana, X., Mar. 1997. Aggregation and breakup of particles in a shear flow. Journal of Colloid and Interface Science 187 (2), 466–473.

Smith, M., Matsoukas, T., 1998. Constant-number Monte Carlo simulation of population balances. Chemical Engineering Science 53 (9), 1777–1786.

Smoluchowski, M. Z., 1917. Versuch einer mathematischen theorie der koagulationskinetik kolloider losunger. Zeitschrift fur Physikalische Chemie 92, 129 – 142.

Vanni, M., 2000. Approximate population balance equations for aggregation-breakage processes. Journal of Colloid and Interface Science 221 (2), 143–160.

Vikas, V., Wang, Z., Passalacqua, A., Fox, R., 2011. Realizable high-order finite-volume schemes for quadrature-based moment methods. Journal of Computational Physics 230 (13), 5328–5352.

Vikas, V., Wang, Z. J., Fox, R. O., 2013. Realizable high-order finite-volume schemes for quadrature-based moment methods applied to diffusion population balance equations. Journal of Computational Physics 249, 162–179.

Weisstein, E. W., 1998. CRC Concise Encyclopedia of Mathematics. CRC Press.

Wheeler, J. C., 1974. Modified moments and Gaussian quadratures. Rocky Mountain Journal of Mathematics 4, 287–296.

Wilck, M., 2001. A general approximation method for solving integrals containing a lognormal weighting function. Journal of Aerosol Science 32 (9), 1111–1116.

Wright, D. L., 2007. Numerical advection of moments of the particle size distribution in eulerian models. Journal of Aerosol Science 38 (3), 352–369.

Yuan, C., Laurent, F., Fox, R., 2012. An extended quadrature method of moments for population balance equations. Journal of Aerosol Science 51, 1–23.

Zhao, H., Maisels, A., Matsoukas, T., Zheng, C., 2007. Analysis of four Monte Carlo methods for the solution of population balances in dispersed systems. Powder Technology 173 (1), 38–50.

Zhao, H., Zheng, C., 2013. A population balance-Monte Carlo method for particle coagulation in spatially inhomogeneous systems. Computers & Fluids 71, 196–207.

List of Figures

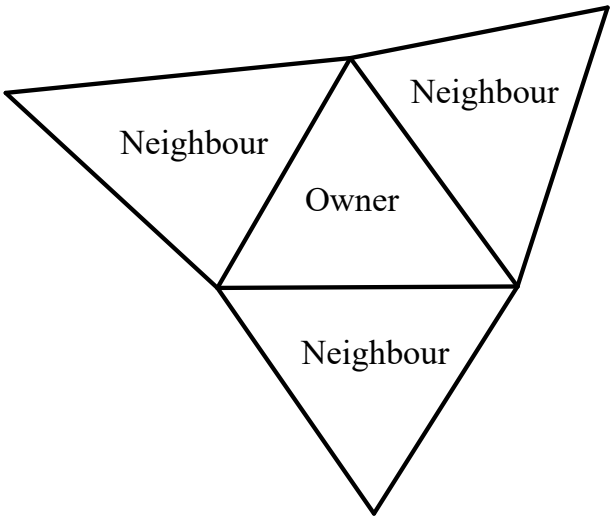

Figure 1: Schematic representation of a computational cell and its neighbour cells, to illustrate the concept of owner and neighbour used in the calculation of moment spatial fluxes.

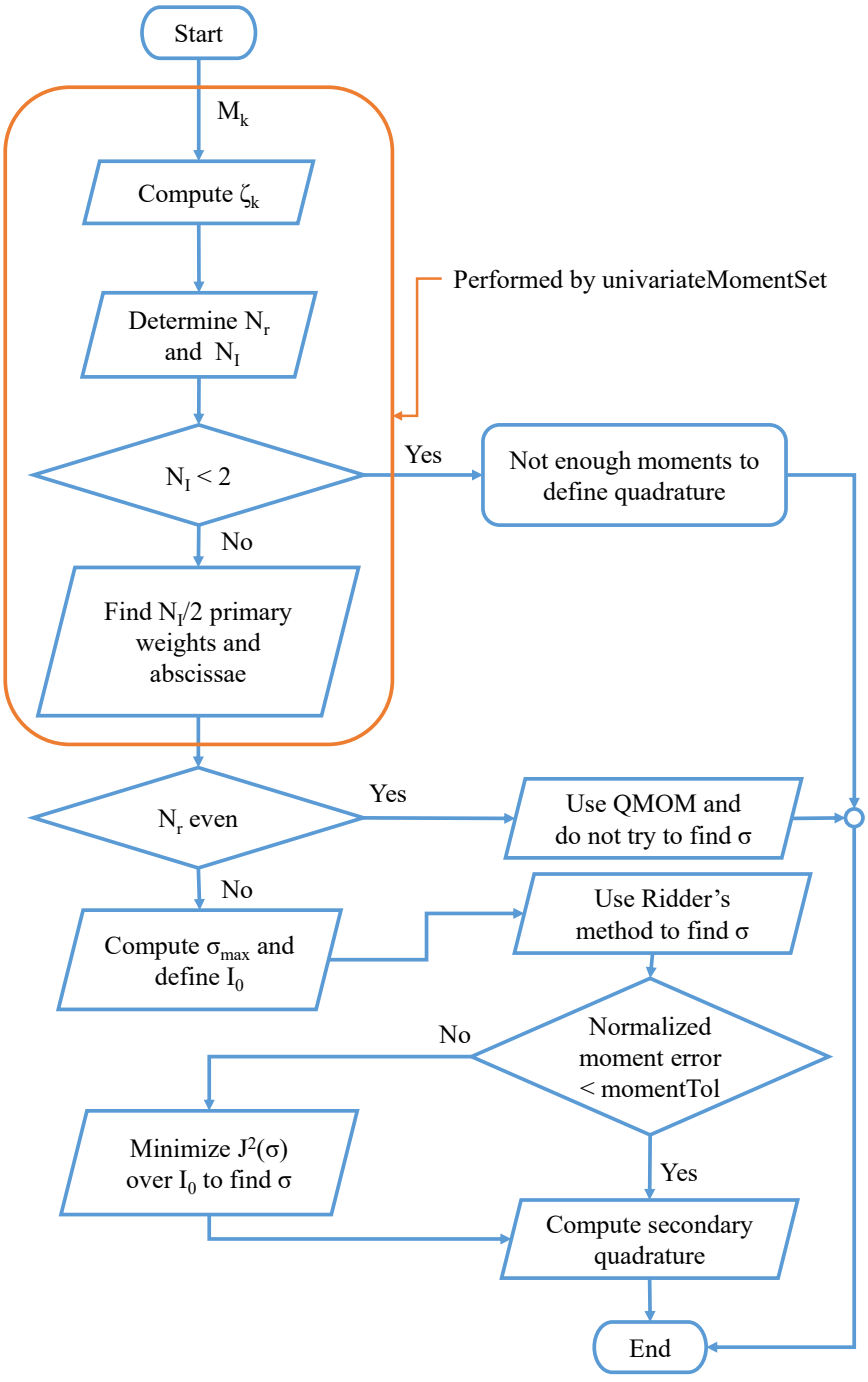

Figure 2: Schematic representation of the EQMOM procedure.

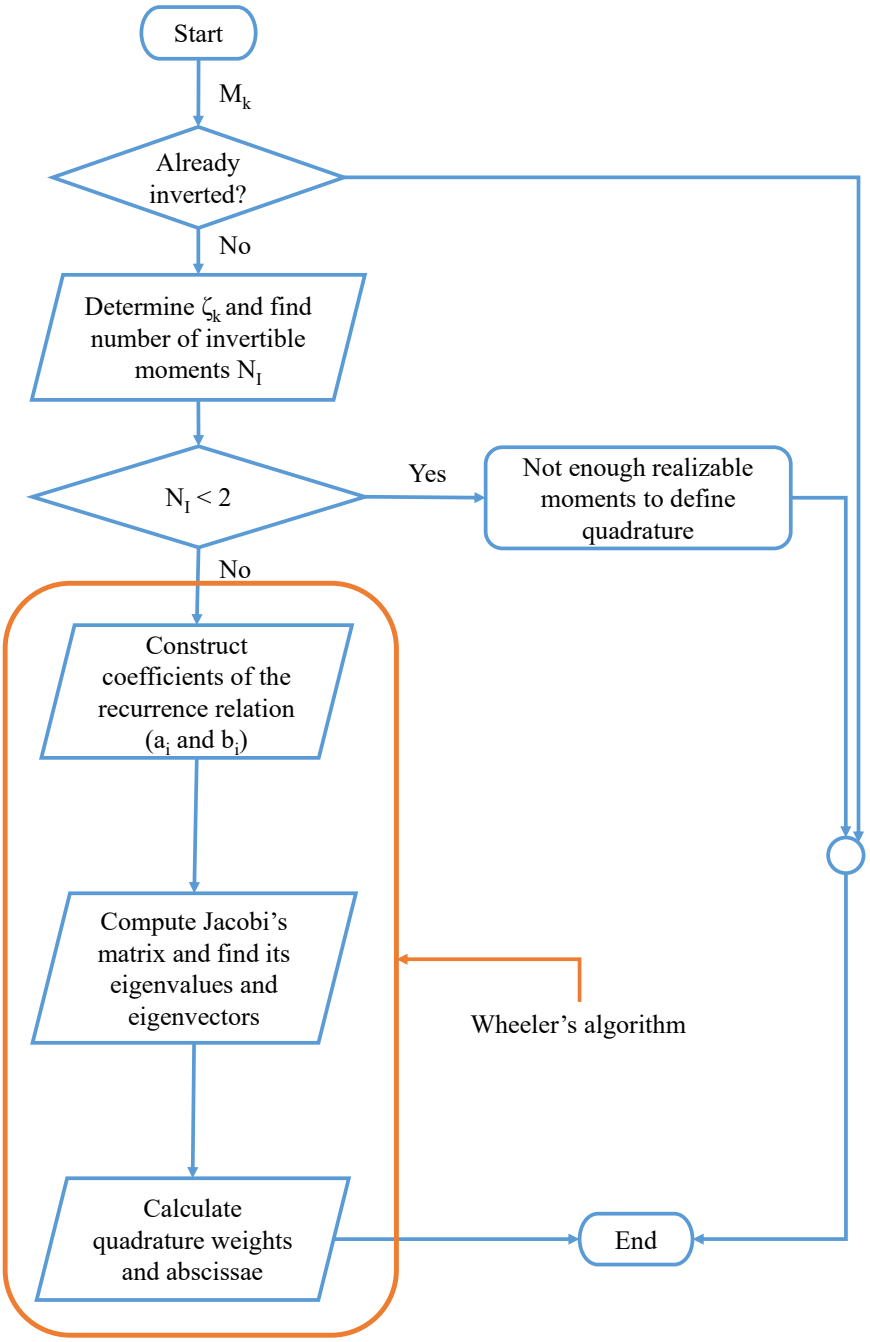

Figure 3: Schematic representation of the ζ_k-Wheeler procedure implemented in the `univariateMomentSet` object.

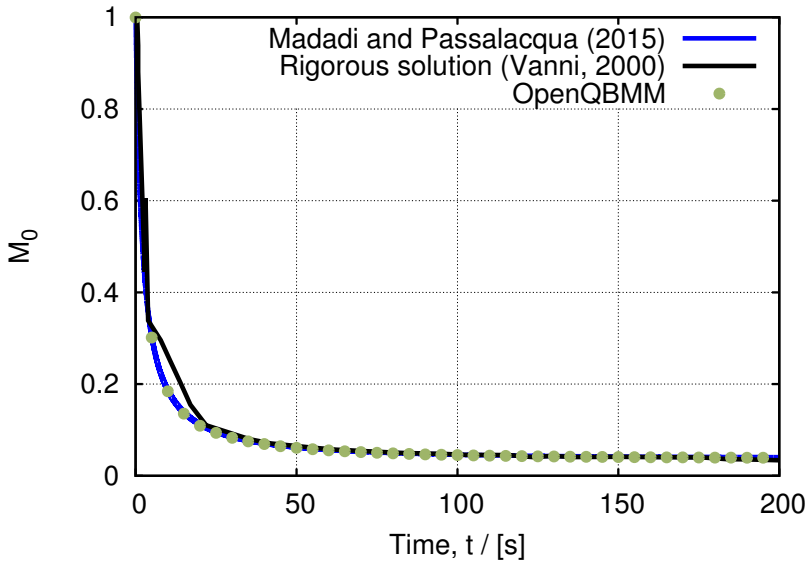

(a) M_0

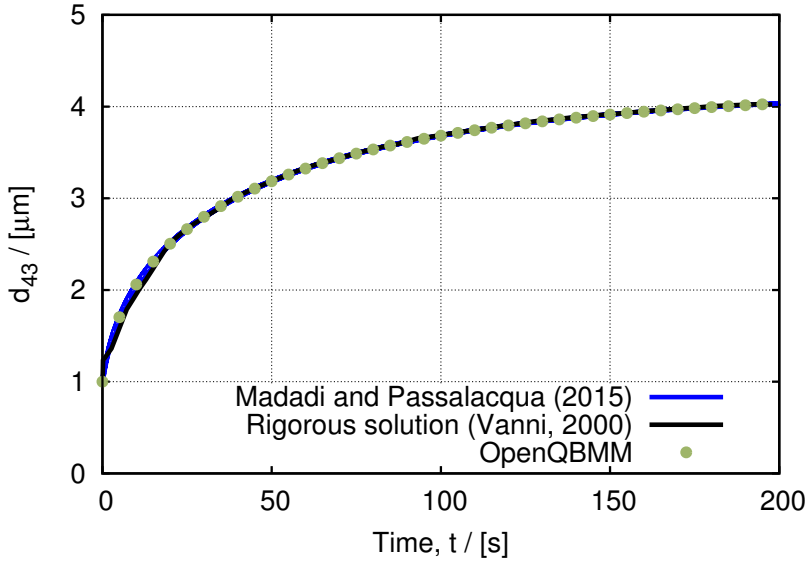

(b) d_{43}

Figure 4: Time evolution of M_0 and of d_{43} in case 1.

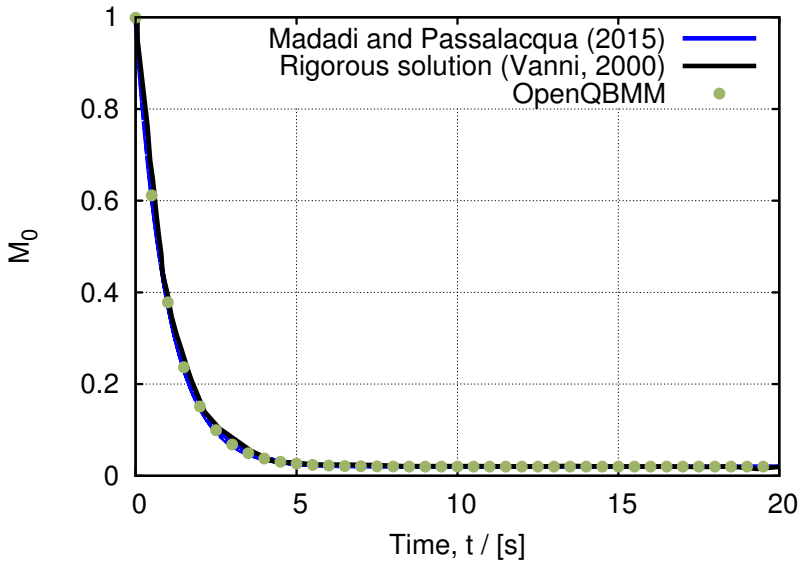

(a) M_0

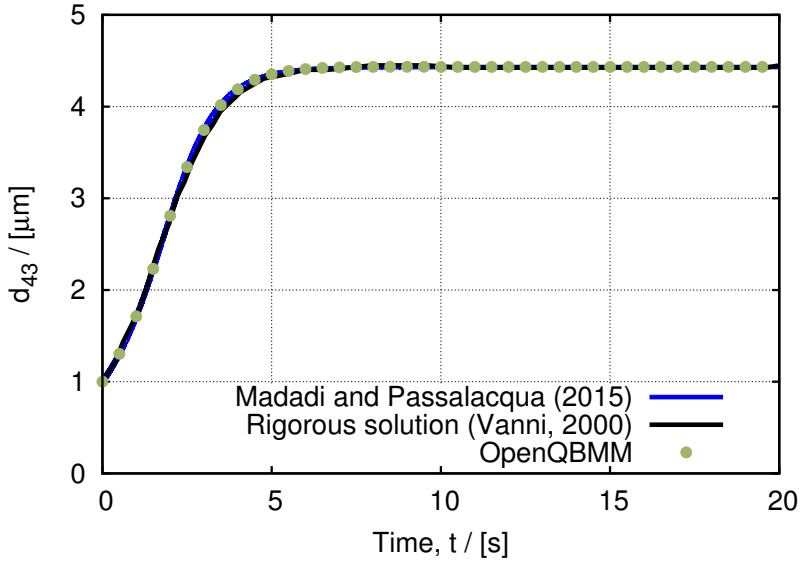

(b) d_{43}

Figure 5: Time evolution of M_0 and of d_{43} in case 2.

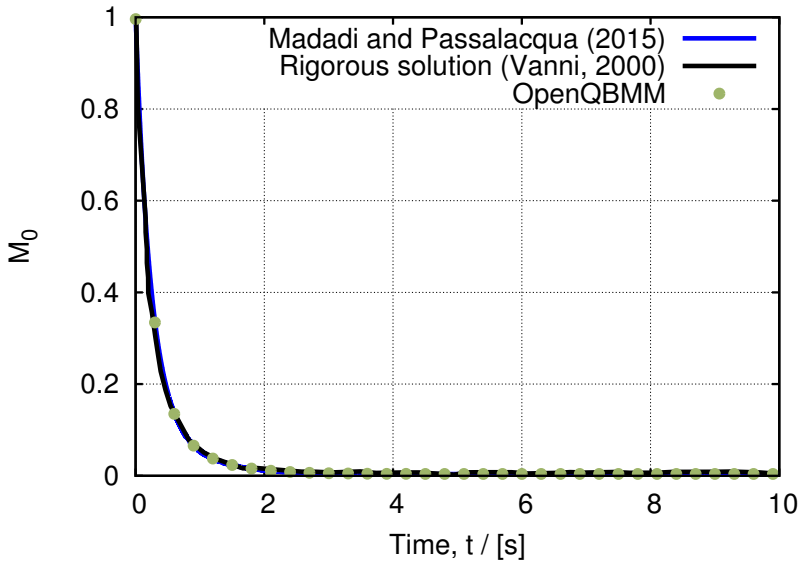

(a) M_0

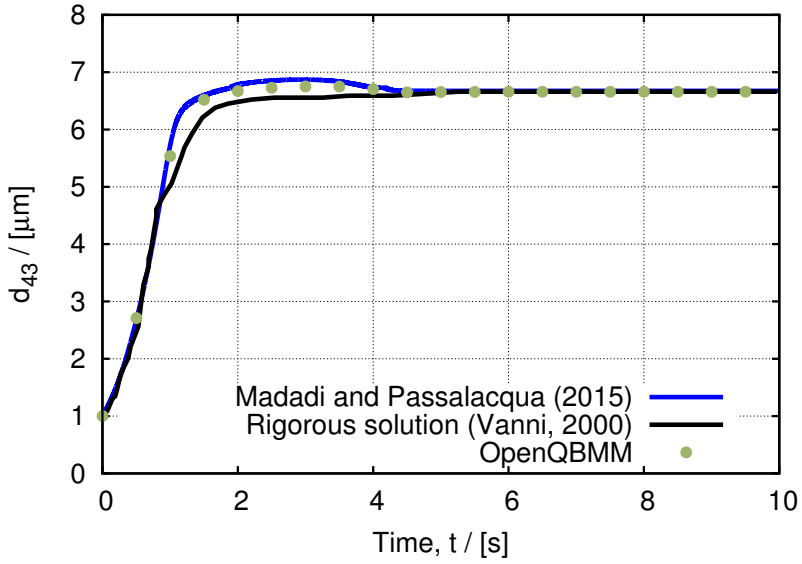

(b) d_{43}

Figure 6: Time evolution of M_0 and of d_{43} in case 3.

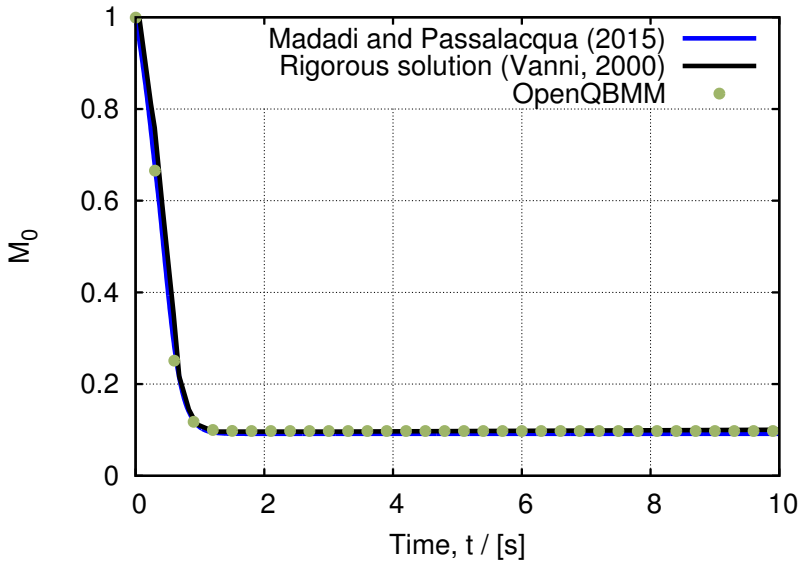

(a) M_0

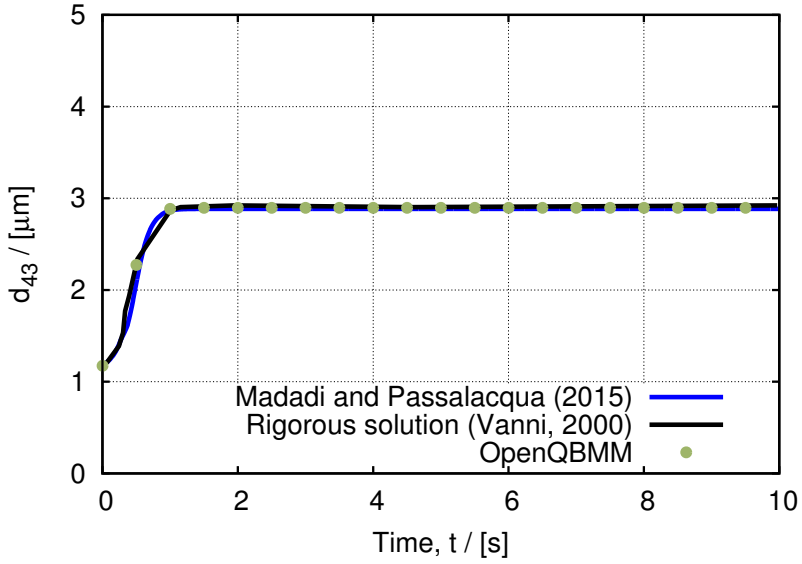

(b) d_{43}

Figure 7: Time evolution of M_0 and of d_{43} in case 4.

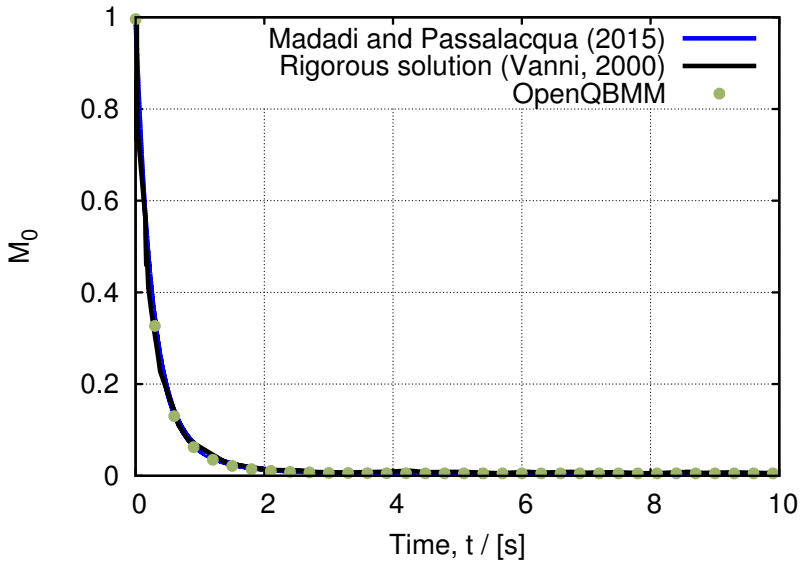

(a) M_0

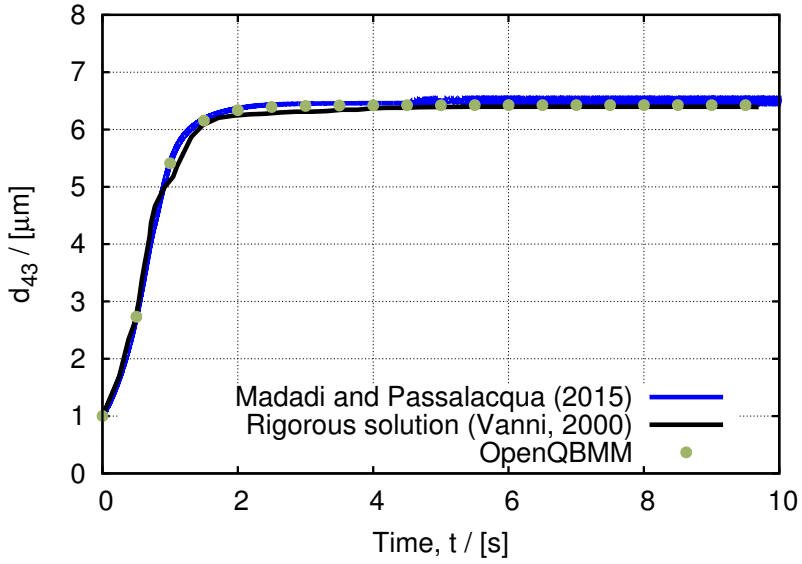

(b) d_{43}

Figure 8: Time evolution of M_0 and of d_{43} in case 5.

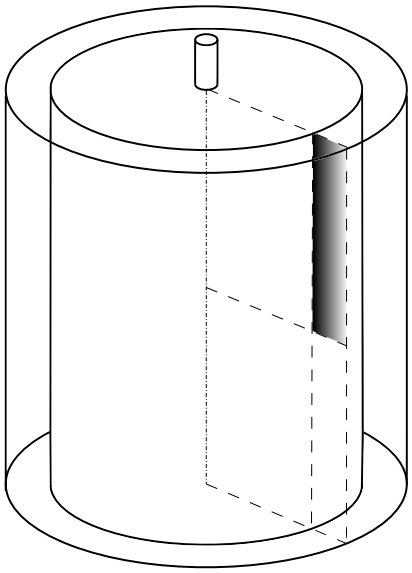

Figure 9: Schematic representation of the Taylor–Couette reactor and of the computational domain used in the simulations.

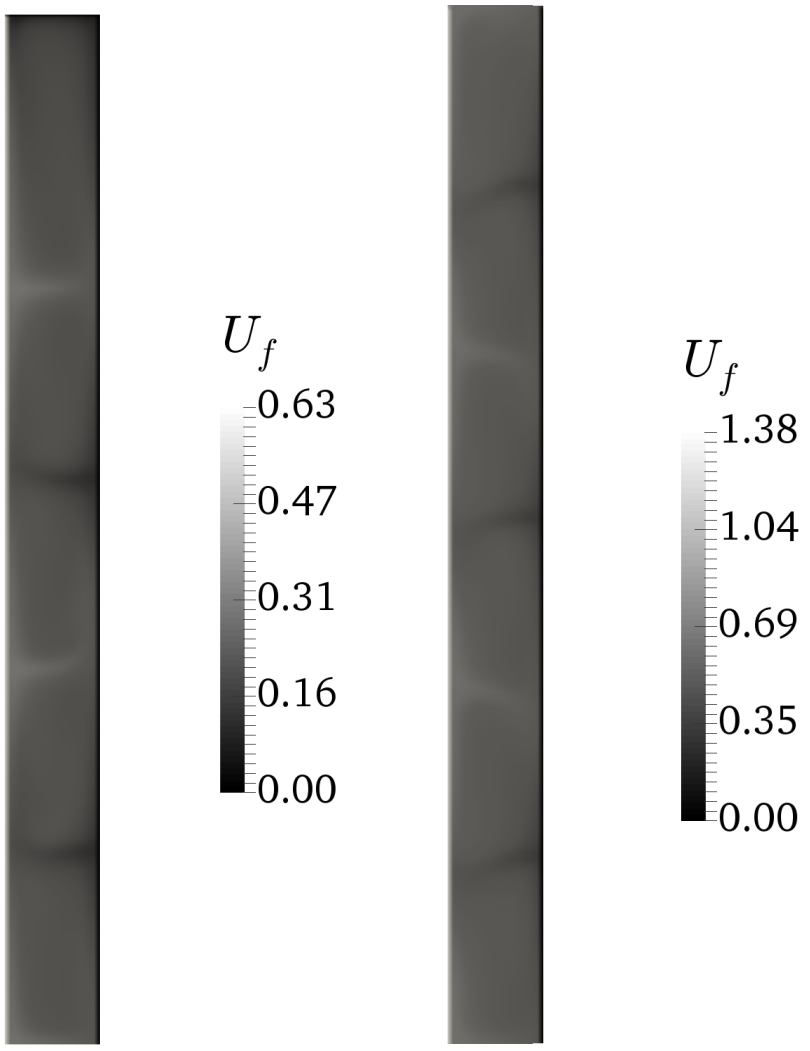

(a) 75 RPM (b) 165 RPM

Figure 10: Velocity magnitude (m/s) of the fluid in the Taylor–Couette reactor.

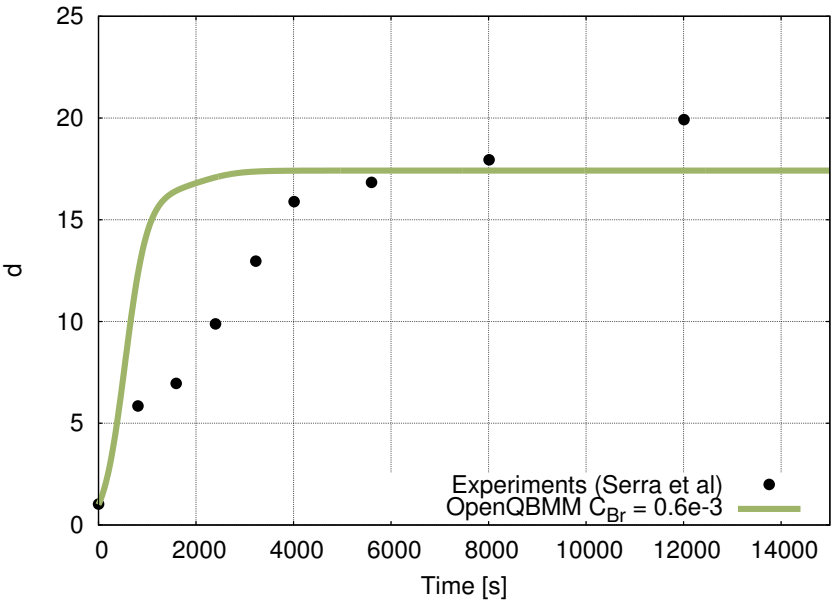

(a) 75 RPM

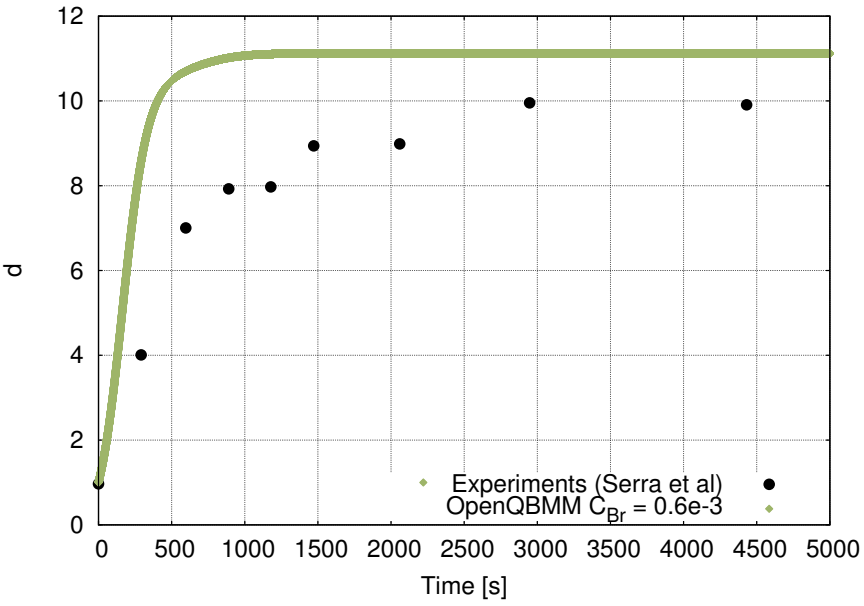

(b) 165 RPM

Figure 11: Time evolution of the volume-average normalized particle diameter in the Taylor–Couette reactor.

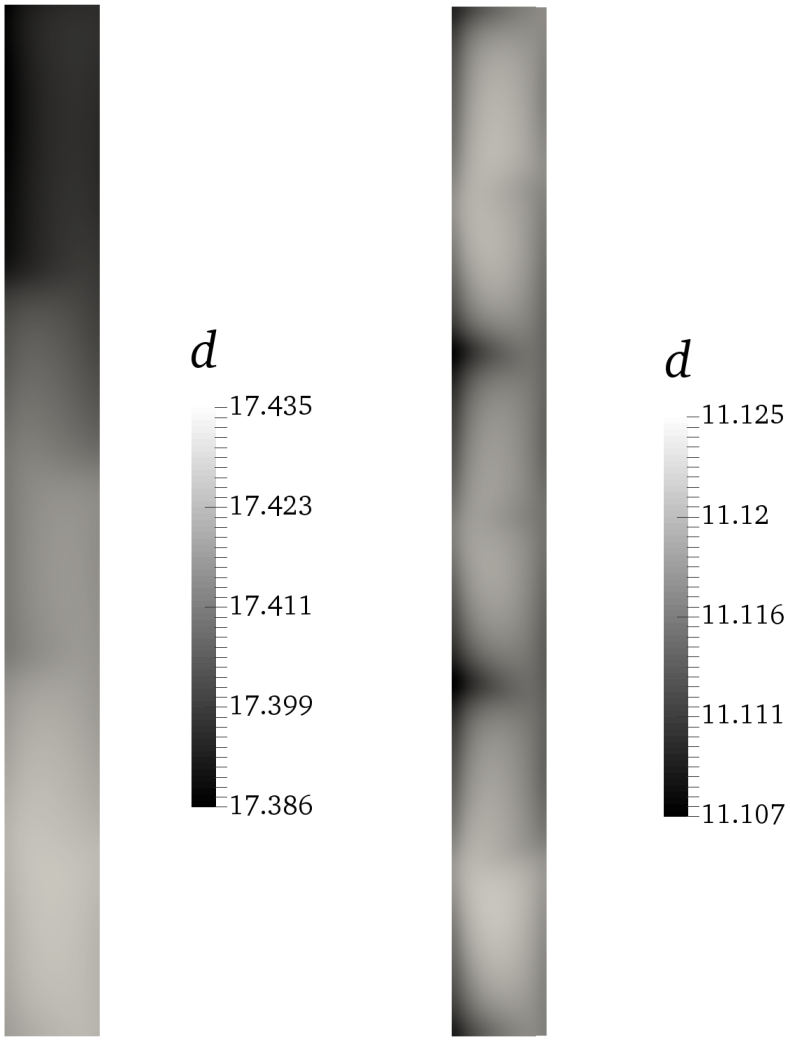

(a) 75 RPM (b) 165 RPM

Figure 12: Steady-state field of the volume-averaged normalized particle diameter in the Taylor–Couette reactor.

List of Tables

Case	N	N_α	$\beta(\xi,\xi')$	$a(\xi)$	$b(\xi\|\xi')$	$M_k(t=0)$
1	2	7	1	$\begin{cases} 0 & \xi = 1 \\ 0.02 & \xi > 1 \end{cases}$	1, Tab. 4	$M_k = 1, k = 0, \ldots, 6$
2	2	7	$\xi^3 + \xi'^3$	$\begin{cases} 0 & \xi = 1 \\ 0.02\xi^3 & \xi > 1 \end{cases}$	1, Tab. 4	$M_k = 1, k = 0, \ldots, 6$
3	2	7	$(\xi + \xi')^3$	$\begin{cases} 0 & \xi = 1 \\ 0.1\,\mathrm{e}^{0.01\xi^3} & \xi > 1 \end{cases}$	1, Tab. 4	$M_k = 1, k = 0, \ldots, 6$
4	3	7	$(\xi + \xi')^2 \lvert\xi^2 - \xi'^2\rvert$	$\begin{cases} 0 & \xi = 1 \\ 0.01\xi^6 & \xi > 1 \end{cases}$	2, Tab. 4	$\begin{cases} M_0 = 1 \\ M_1 = 1.13 \\ M_2 = 1.294 \\ M_3 = 1.5 \\ M_4 = 1.760 \\ M_5 = 2.087 \\ M_6 = 2.087 \end{cases}$
5	4	10	$(\xi + \xi')^3$	$\begin{cases} 0 & \xi < \sqrt[3]{5} \\ 0.1\,\mathrm{e}^{0.01\xi^3} & \xi \geq \sqrt[3]{5} \end{cases}$	3, Tab. 4	$M_k = 1, k = 0, \ldots, 6$

Table 1: Cases examined for the aggregation and breakage process.

Kernel	$\beta(\xi, \xi')$
Constant	1
Sum	$\xi^3 + \xi'^3$
Hydrodynamic	$(\xi + \xi')^3$
Differential force	$(\xi + \xi')^2 \lvert\xi^2 - \xi'^2\rvert$

Table 2: Aggregation kernels.

Kernel	$a(\xi)$
Constant	1
Power law	ξ^{α}
Exponential	$\mathrm{e}^{\delta\xi^3}$

Table 3: Breakage kernels.

No.	Mechanism	$b\left(\xi\middle\vert\xi'\right)$	$\bar{b}^k$
1	Symmetric fragmentation	$\begin{cases} 2 & \xi = \xi'/2^{1/3} \\ 0 & \text{otherwise} \end{cases}$	$2^{(3-k)/3}\xi^k$
2	Uniform	$\begin{cases} 6\xi^2/\xi'^3 & \xi \in]0, \xi'[\\ 0 & \text{otherwise} \end{cases}$	$6\xi^k/(k+3)$
3	Mass ratio 1 to 4	$\begin{cases} 1 & \xi = \xi' \left(\frac{1}{5}\right)^{1/3} \\ 1 & \xi = \xi' \left(\frac{4}{5}\right)^{1/3} \\ 0 & \text{otherwise} \end{cases}$	$\xi^k \frac{4^{k/3}+1}{5^{k/3}}$

Table 4: Daughter distribution functions and their moment transformations.